Designing Optimal Linear Detectors: A Bottom-Up Approach

Joe Bentley,[1,*] Hendra Nurdin,[2] Yanbei Chen,[3] Xiang Li,[3] and Haixing Miao[1]

[1] *Institute for Gravitational Wave Astronomy, School of Physics and Astronomy, University of Birmingham, Birmingham B15 2TT, United Kingdom*

[2] *School of Electrical Engineering and Telecommunications, University of New South Wales, Sydney 2052, Australia*

[3] *Theoretical Astrophysics 350-17, California Institute of Technology, Pasadena, California 91125, USA*

(Received 18 October 2021; revised 2 February 2022; accepted 2 February 2023; published 2 March 2023)

This paper develops a systematic approach to realizing linear detectors with an optimized sensitivity, allowing for the detection of extremely weak signals. First, general constraints are derived on a specific class of input-output transfer functions of a linear detector. Then a physical realization of transfer functions in that class is found using the quantum network synthesis technique, which allows for the inference of the physical setup directly from the input-output transfer function. By exploring a minimal realization which has the minimum number of internal modes, it is shown that the optimal such detectors are internal squeezing schemes. Then, investigating nonminimal realizations, which is motivated by parity-time symmetric systems, a quantum nondemolition measurement is systematically recovered.

DOI: 10.1103/PhysRevApplied.19.034009

I. INTRODUCTION

The sensitivity of high-precision optical measurements, such as those performed in advanced gravitational wave (GW) detectors [1,2], is ultimately limited by the fundamental fluctuations of the quantum vacuum, known as the quantum noise. For GW detectors, increasing the quantum-noise-limited sensitivity will allow us to detect sources arising from a greater volume of the universe, as well the full neutron star inspiral waveform, allowing the determination of the neutron star equation of state [3,4]. The sensitivity of linear detectors is ultimately constrained by the quantum Cramér-Rao bound (QCRB) which states that the variance of the measured signal due to noise is inversely proportional the variance σ_{NN} of the photon number of the probe degree of freedom coupled to the signal [5–10]. For vacuum or coherent (laser) states of light, this quantity is ultimately limited by the Heisenberg limit $\sigma_{NN} \sim N^2$, which states that the uncertainty scales quadratically with the number of resources available (for optical detectors N is the mean number of photons in the probe degree of freedom), although for most resonant detectors it is often constrained by the stronger shot-noise limit (also called the standard quantum limit in quantum metrology): $\sigma_{NN} = N$ [11]. This shot-noise limit can be surpassed using techniques such as bandwidth broadening via negative dispersion [12–15]; however, in this case the Heisenberg limit is not saturated since σ_{NN} is explicitly bounded to a value less than N^2. Previously the Heisenberg limit for phase measurement has been saturated in a nonresonant detector using a combination of entanglement, multiple sampling, and probabilistic adaptive measurements [16]. Theoretical examples of systems that saturate the limit have also been derived for exotic nonclassical states [17,18] and using quantum error correction [19]. Here we instead focus on linear optical phase measurement, and focus on maximizing σ_{NN}; however, we cannot claim to saturate the Heisenberg limit due to our approximation of a linearized coupling of the signal to the detector. We call a linear detector with a maximal σ_{NN} an *optimal linear detector* since, as we will see, it also optimizes the sensitivity to a linearly coupled classical signal. In this paper we then introduce a general approach to realizing an optimal linear detector directly from its input-output transfer function.

A brief outline of the approach is as follows. First, we start with a physically realizable transfer function with order n in frequency. This order sets a limit on the complexity of the system, since the corresponding physical realization will have a number of internal modes limited by this order. Then, from this realization, we investigate to which internal mode a signal should be coupled in order to gain a maximum signal-to-noise ratio, corresponding to the internal mode to which the input vacuum fluctuations have the maximum coupling, thus giving an optimal nth-order detector.

This approach leads to both minimal and nonminimal realizations: the minimal realization of a first-order transfer function that is active (has nonunity gain) exhibits

*Corresponding author: joe.bentley@uni-hamburg.de

internal squeezing, directly increasing the photon number fluctuation in the probe degree of freedom, as explored in [20–22]; the nonminimal realization begins with the minimal realization of a first-order lossless passive detector that is shot-noise-limited, then adds a pair of auxiliary modes that result in an infinite signal amplification at dc (i.e., for low-frequency signals). The latter is motivated by the parity-time (*PT*) symmetric system explored in [23,24]. In both cases, we use the systematic realization framework developed in [25] to realize the simplest single-degree-of-freedom system with squeezing, which can be extended to arbitrarily many degrees-of-freedom using this framework. For the signal amplification case, the input-output relation must remain the same so that additional noise channels are not added, and we derive the corresponding conditions for modifying a system's internal dynamics without affecting its input-output transfer function. Additionally we show that this is related to an ideal quantum nondemolition (QND) measurement [26,27], and quantum-mechanics-free subsystems ([28, §III], [29, Appendix D], [30,31]). Further, we show how the dynamics can be arbitrarily modified by adding additional hidden modes while maintaining the QND property of the variable, for example so that the detector's most sensitive frequency can be tuned to a specific frequency, not limited to dc. As discussed, in all cases we start with the system's transfer function, since the order of a system's input-output transfer function determines the complexity of the minimal realization of the system, specifically determining the number of internal degrees of freedom of the system [32]. In this way we can then start with full control on the complexity of the resulting detector in the design process.

The outline of this paper is as follows. In Sec. II we define the transfer function used to analyze the linear systems in this paper. In Sec. III we show how quantum network synthesis can be used to find a physical realization directly from the transfer function, and how the resulting detector's performance can be evaluated using the QCRB. In Sec. IV we then discuss the various conditions on the transfer function arising from the physical realizability conditions, which specifies the number of parameters needed to describe a physically realizable system. In Sec. V we consider the optimal minimal realization of the first-order transfer function, showing that it is an internal squeezing scheme. In Sec. VI we consider the optimal nonminimal by augmenting a shot-noise-limited tuned cavity with auxiliary modes that do not affect the input-output dynamics, leading to a saturated signal amplification, and further that an ideal QND measurement is realized. It must be stressed that in both cases the infinite signal response arises from the approximations of our analysis, which breaks down as the uncertainty becomes comparable to the mean, and therefore we cannot infer that we completely reach the Heisenberg limit.

II. THE TRANSFER FUNCTION OF LINEAR SYSTEMS

In this work we are concerned with quantum systems with linear dynamics in the Heisenberg picture [33]. In this section we briefly review some of the relevant concepts, with further details deferred to Appendix A. We consider finite-dimensional linear quantum systems (in the sense that there are only a finite number of internal modes) with their dynamics given in the general form

$$\begin{aligned} \dot{\mathbf{x}} &= A\mathbf{x} + B\mathbf{u}, \\ \mathbf{y} &= C\mathbf{x} + D\mathbf{u}, \end{aligned} \tag{1}$$

where $\mathbf{x}$ is a column vector containing the operators for the internal modes, $\mathbf{u}$ is a column vector of input operators to the system, and $\mathbf{y}$ is column vector of output operators from the system; A, B, C, and D are complex matrices of the appropriate dimensions compatible with $\mathbf{u}$, $\mathbf{x}$, and $\mathbf{y}$. In particular, A is a square matrix. More generally, A, B, C, and D could potentially be integro-differential operators rather than constant matrices. In some cases this may be rewritten in the form (1) by introducing a finite number of additional degrees of freedom. However, in general it may be necessary to introduce an infinite number of additional degrees of freedom, corresponding to A, B, C, and D having an infinite number of rows and columns. An example is a model of linear gradient echo memories considered in [34], a model involving continuous spatial degrees of freedom. For the purposes of this work, we are interested solely in the finite-dimensional case as given by (1).

In this paper we restrict the analysis to single-input, single-output quantum systems with the input and output fields each described by a pair of bosonic annihilation and creation operators or quadratures in the two-photon formalism described by Caves and Schumaker [35,36]. The output $\mathbf{y}$ has the decomposition $\mathbf{y} = \mathbf{y}_n + \mathbf{y}_f$, where $\mathbf{y}_n$ and $\mathbf{y}_f$ are the natural response and forced response, respectively, given by

$$\begin{aligned} \mathbf{y}_n(t) &= \mathrm{C}e^{At}\mathbf{x}(0^-), \\ \mathbf{y}_f(t) &= \int_{0^-}^{t} \mathrm{C}e^{A(t-\tau)}B\mathbf{u}(\tau)d\tau + D\mathbf{u}(t), \end{aligned}$$

where $\mathbf{x}(0^-)$ is the initial condition for x at time $t = 0^-$ just before $t = 0$. The natural response only depends on the initial condition $\mathbf{x}(0^-)$ but not the input $\mathbf{u}$, while the forced response is the system's output response to the input $\mathbf{u}$ and does not depend on $\mathbf{x}(0^-)$.

For causal systems, the impulse response or Green's function h for the system is given by $h(t) = \mathrm{C}e^{At}B\,\Theta(t) + D\delta(t)$, where $\Theta(t)$ is the Heaviside step function and $\delta(t)$ is the Dirac delta function. Note that $\mathbf{y}_f$ is the convolution of h with $\mathbf{u}$. If $h(t) = O(e^{\sigma t})$ then the system's transfer function is a complex function defined by

$$H(\Omega) = \int_{0^-}^{\infty} h(t) e^{i\Omega t} dt, \quad \mathrm{Im}\{\Omega\} > \sigma. \tag{2}$$

To conclude this section, we note that the transfer function coincides with the unilateral (one-sided) Laplace transform $\mathcal{L}[h](s) = \int_{0^-}^{\infty} h(t)e^{st}dt$ of h with the identification $s = i\Omega$ (note that in many fields, for example in engineering as in [37] and [33, Chapter 2], the Laplace transform is defined with s replaced by $-s$).

III. QUANTUM CRAMÉR-RAO BOUND

In this section we show how an optimal detector can be engineered by minimizing the QCRB [9]. This is performed by engineering diverging transfer functions from the vacuum input to the probe degree of freedom. As stressed previously, any divergent response we engineer is a result of our approximations of a linear signal coupling, as well as a more specific approximation arising from the specific physical realization of each system which we will treat as we come to them.

The QCRB sets a lower limit on the variance of an unbiased estimator of a classical signal $x_c(t)$ coupled to a detector linearly via $\hat{H}_{\mathrm{int}} = -\hat{F}x_c(t)$,

$$S_{xx}(\Omega) > \frac{\hbar^2}{S_{FF}(\Omega)} \equiv \sigma_{xx}^{\mathrm{QCRB}}(\Omega), \tag{3}$$

where $S_{xx}(\Omega)$ is the single-sided displacement power spectral density and $S_{FF}(\Omega)$ is the spectral density describing the quantum fluctuations of the degree of freedom $\hat{F}$ that couples to the classical signal. In this paper we consider lossless systems, and so the spectral density of $\hat{F}$ is given by

$$S_{FF}(\Omega) = S_{uu}(\Omega)|G_{uF}(\Omega)|^2 = |G_{uF}(\Omega)|^2, \tag{4}$$

where $G_{uF}(\Omega)$ is the open-loop transfer function from the input $\hat{u}$ to the internal degree of freedom $\hat{F}$ which belongs to the vector of internal modes $\mathbf{x}$. With external squeezing we decrease the QCRB by increasing $S_{uu}(\Omega)$ which is a well-known technique, so here we have restricted the input to a unsqueezed vacuum input: $S_{uu}(\Omega) = 1$.

We illustrate the general process using an optical interferometer with Fabry-Pérot cavities which detects small modulations of the cavity lengths $x_c(t) = \Delta L(t)$, equivalent to differential displacement of the mirrors [38]. In this case, after linearizing the radiation pressure force of the light on the mirrors (as discussed in Sec. V), we arrive at a linear coupling of this length modulation to the amplitude quadrature of the cavity, so that the probe degree of freedom is $\hat{F} \propto \hat{a}^1 \equiv \hat{a} + \hat{a}^\dagger$, where $\hat{a}$ is the annihilation operator of the cavity mode. Here the probe fluctuation is related to the intracavity photon number fluctuation by

$$S_{FF}(\Omega) = |G_{uF}(\Omega)|^2 = \frac{\hbar^2\omega_0^2}{L^2} S_{NN}(\Omega), \tag{5}$$

where $S_{NN}(\Omega)$ is the spectral density describing the photon number fluctuations, ω_0 is the laser carrier frequency, and L is the arm cavity length. In this case we measure the displacement $x_c(t)$ and therefore a good figure of merit is the signal-to-noise ratio,

$$\mathrm{SNR} = \int_0^{\infty} \frac{d\Omega}{2\pi} \frac{|x_c(\Omega)|^2}{S_{xx}(\Omega)}, \tag{6}$$

where $x_c(\Omega)$ is the Fourier transform of the classical signal. For a displacement spectrum that is flat (frequency independent: $|x_c(\Omega)| = |x_c|$), this SNR is bound by the QCRB,

$$\begin{aligned} \mathrm{SNR} &\leq \int_0^{\infty} \frac{d\Omega}{2\pi} \frac{|x_c|^2}{\sigma_{xx}^{\mathrm{QCRB}}(\Omega)} \\ &= \frac{|x_c|^2}{\hbar^2} \int_0^{\infty} \frac{d\Omega}{2\pi} |G_{uF}(\Omega)|^2 = \frac{\omega_0^2 |x_c|^2}{L^2} \sigma_{NN}, \end{aligned} \tag{7}$$

and σ_{NN} is total variance of the photon number of the probe degree of freedom. Therefore by maximizing $|G_{uF}(\Omega)|^2$, we maximize the probe fluctuation $S_{FF}(\Omega)$ and the photon number variance σ_{NN}, therefore minimizing the QCRB and maximizing the SNR.

The general approach for realizing an optimal detector is then performed as follows. First, as shown in [25], we can synthesize any n-degree-of-freedom system directly from its input-output transfer function, so long as it obeys certain conditions which is discussed in Sec. IV. Then, labeling each internal degree of freedom of the realization as $\hat{F}_i$, $i = 1, \ldots, n$, we can calculate the open-loop transfer functions from the input to those degrees of freedom, $G_{uF_i}(\Omega)$. Finally, we can maximize the right-hand side of Eq. (7) by maximizing $G_{uF_i}(\Omega)$ for the optimal system parameters and also choosing the optimal internal degree of freedom $\hat{F}_i$ to which to couple the signal $x(t)$, giving us a systematic way of optimizing the detector design given the input-output transfer function.

IV. GENERAL CONSTRAINTS ON THE INPUT-OUTPUT RELATIONS OF LINEAR DETECTORS

In this section we derive some general constraints on a certain class of transfer functions by investigating their physical realizability. We do this by investigating whether or not they can lead to dynamics that preserve the commutation relations of the input-output operators [28,37].

In this work we consider a class of quadrature-picture rational transfer functions (i.e., with scalar rational transfer

functions as entries) that can be transformed into diagonal form with rational entries through multiplication by unitary transfer functions on the left and on the right. However, in doing this we lose some generality, since not all transfer functions can be transformed into this form. In general, one can transform transfer functions into a diagonal form with nonrational entries (by applying the symplectic decomposition in [39] to each value of Ω). Nonetheless, nonrational transfer functions can be approximated arbitrary closely with rational transfer functions by using methods such as Padé approximation [40] and requiring that the approximation satisfy the physical realizability condition (11) below.

Let $\hat{y}^{1,2}$ and $\hat{u}^{1,2}$ be the output and input fields respectively in the two-photon quadrature formalism [35,36]. Then they are related by a transfer function $\mathbf{G}_q$ (a $\mathbb{C}^{2\times 2}$-valued complex function) as

$$\begin{bmatrix}\hat{y}_1(\Omega)\\ \hat{y}_2(\Omega)\end{bmatrix} = \mathbf{G}_q(\Omega)\begin{bmatrix}\hat{u}_1(\Omega)\\ \hat{u}_2(\Omega)\end{bmatrix}, \tag{8}$$

where, as mentioned, we assume $\mathbf{G}_q$ to be a diagonal matrix with rational elements,

$$\mathbf{G}_q(\Omega) = \begin{bmatrix}G_{11}(\Omega) & 0\\ 0 & G_{22}(\Omega)\end{bmatrix}. \tag{9}$$

One special case is where $|G_{11}(\Omega)|^2 = |G_{22}(\Omega)|^2 = 1$, in which case we have no squeezing (see Sec. VI). To parameterize the transfer function, we consider an n-degree-of-freedom pole-zero form,

$$G_{11}(\Omega) = \frac{\prod_{j=1}^{n}(i\Omega - z_j)}{\prod_{k=1}^{n}(i\Omega - p_k)}, \tag{10}$$

where $\{z_j \in \mathbb{C} \mid j = 1,\dots,n\}$ and $\{p_k \in \mathbb{C} \mid k = 1,\dots,n\}$ are the zeros and poles respectively, without any element in common between the zeros and poles. The expansion to n is chosen as the minimal state-space realization of an nth-order pole-zero transfer function in this case will have n internal modes, setting a limit on the complexity of the resulting realization; however, applying the realization framework may result in additional auxiliary modes [25]. As shown in [37], the transfer function is physically realizable if

$$\mathbf{G}_q^{\dagger}(-\Omega^*)\Theta\mathbf{G}_q(-\Omega) = \Theta, \tag{11}$$

and

$$\Theta = \begin{bmatrix}0 & i\\ -i & 0\end{bmatrix}, \tag{12}$$

which up to a factor of i is the simplest matrix that takes part in the symplectic condition. This condition restricts the conjugate transfer function to

$$G_{22}(\Omega) = \frac{\prod_{k=1}^{n}(-i\Omega - p_k^*)}{\prod_{j=1}^{n}(-i\Omega - z_j^*)}, \tag{13}$$

and so the poles/zeroes of G_{22} are the conjugates of the zeroes/poles of G_{11} respectively and the sign of the frequency is flipped. Since the real and imaginary parts of the poles and zeroes are independent we have in total $4n$ independent parameters specifying our system.

The possible poles and zeroes can be further reduced by noting that the quadrature operators are real in the time domain and so the transfer function must obey $\mathbf{G}_q(-\Omega) = \mathbf{G}_q^{\dagger}(\Omega)$, which leads to the equation

$$\prod_{j,k=1}^{n}(-i\Omega - p_k)(i\Omega - z_j^*) = \prod_{j,k=1}^{n}(i\Omega - p_k^*)(-i\Omega - z_j), \tag{14}$$

which can be expanded as

$$\sum_{j=1}^{2n} a_j\,(i\Omega)^{j-1} = 0, \tag{15}$$

where a_j are algebraic combinations of the poles and zeros. Therefore we have $a_j = 0$, $j = 1,\dots,2n$, and the number of independent parameters is reduced to $2n$.

V. INTERNAL SQUEEZING

In this section we consider the minimal realization of a first-order input-output transfer function exhibiting squeezing, that is, $|G(\Omega)| \neq 1$ for the quadrature operators, and the off-diagonal terms are nonzero for the sideband operators. We will see that the internal squeezing schemes are optimal for a classical signal coupled linearly to the cavity mode. We will choose the classical signal to be a displacement of the cavity length, as discussed in Sec. III, although the analysis is general to linear detectors. According to the previous section, the most general first-order transfer function that is rational is quantified by two independent real parameters, and is given in the quadrature picture by

$$\mathbf{G}^q(\Omega) = \begin{bmatrix}\dfrac{\alpha + i\Omega}{\beta - i\Omega} & 0\\ 0 & \dfrac{\beta + i\Omega}{\alpha - i\Omega}\end{bmatrix}, \tag{16}$$

which obeys Eq. (11). In Appendix B we derive the physically realizable state space directly from the above transfer

function, giving

$$A = \frac{1}{2}\begin{bmatrix} -\alpha-\beta & \alpha-\beta \\ \alpha-\beta & -\alpha-\beta \end{bmatrix},$$
$$B = \sqrt{\alpha+\beta}\, I_{2\times 2}, \tag{17}$$
$$C = -\sqrt{\alpha+\beta}\, I_{2\times 2}, \quad D = I_{2\times 2}.$$

The physical realization of this system, shown in Fig. 1, has one internal degree of freedom and in the generalized open oscillator formalism (discussed extensively in [32]) is given by

$$S = I_{2\times 2}, \tag{18}$$
$$\hat{L} = \sqrt{\alpha+\beta}\,\hat{a}, \tag{19}$$
$$\hat{H} = -\frac{i}{4}\hbar(\alpha-\beta)(\hat{a}\hat{a} - \hat{a}^\dagger\hat{a}^\dagger), \tag{20}$$

where $\hat{a}$ is the annihilation operator of the cavity mode. Here S is the input-output direct scattering matrix, $\hat{L}$ is the coupling operator to the external continuum, and $\hat{H}$ is the system's internal Hamiltonian in the rotating frame at the laser carrier frequency. As shown in [25], this corresponds to a tuned cavity with coupling coefficient $\gamma \equiv (\alpha+\beta)/2$ containing a nonlinear crystal with coupling frequency $\chi \equiv (\alpha-\beta)/2$, which is related to the single-pass squeezing factor by $r = 2\chi L/c$ where L is the cavity length. Inverting these relations gives $\alpha = \gamma + \chi$ and $\beta = \gamma - \chi$.

The quadrature picture transfer function from the inputs to the internal degree of freedom is given by

$$\begin{bmatrix} \hat{a}^1 \\ \hat{a}^2 \end{bmatrix} = \begin{bmatrix} \dfrac{\sqrt{2\gamma}}{\gamma-\chi-i\Omega} & 0 \\ 0 & \dfrac{\sqrt{2\gamma}}{\gamma+\chi-i\Omega} \end{bmatrix} \begin{bmatrix} \hat{a}^1_{\rm in} \\ \hat{a}^2_{\rm in} \end{bmatrix}. \tag{21}$$

In this case, the classical signal x_c, whose variance is lower-bounded by the QCRB in Eq. (3), is the length modulation of the cavity, and is coupled to the probe degree of freedom linearly. This probe degree of freedom is, in turn, proportional to the probe amplitude quadrature $\hat{a}^1$.

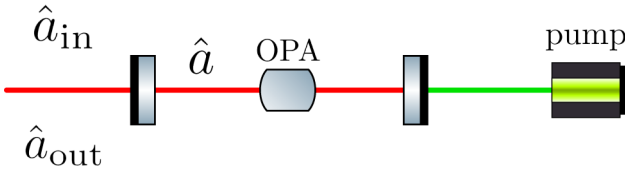

FIG. 1. The setup for the squeezing of one quadrature via internal squeezing within the cavity, achieving an SNR that diverges at dc. The optical parametric amplifier (OPA) is pumped by the classical pump beam.

The linear coupling requires the application of a linearization procedure of the radiation pressure as performed in [41], which specifically requires that any fluctuations of the field are much smaller than the mean. Fixing the proportional constant (the actual value does not affect the optimization), we have $\hat{F} \equiv (\hbar\omega_0\sqrt{2N}/L)\hat{a}^1$ with N the mean photon number and the input field is $\hat{u} \equiv \hat{a}^1_{\rm in}$, giving the input-to-probe transfer function

$$G_{uF}(\Omega) = \left(\frac{\hbar\omega_0\sqrt{2N}}{L}\right)\frac{\sqrt{2\gamma}}{\gamma-\chi-i\Omega}. \tag{22}$$

The probe photon fluctuation is given by the integral in Eq. (7),

$$\sigma_{NN} = 2N\int_0^\infty \frac{d\Omega}{2\pi}\frac{2\gamma}{|\gamma-\chi-i\Omega|^2}. \tag{23}$$

Clearly at $\gamma = \chi$ the integrand diverges at $\Omega = 0$ and thus the total probe fluctuation will diverge, corresponding to an increase in the signal response. As stressed previously, the probe fluctuation is only valid up to the point where it approaches the mean. This corresponds to the threshold case where the cavity acts as an optical parametric oscillator, since the damping of the cavity mode exactly compensates the pumping due to the nonlinear crystal interaction. We have made the approximation that the pump will never be depleted; in practice, as γ approaches χ, the latter will always change due to the decrease in pump power. At $\gamma \neq \chi$ the integral is solved trivially as

$$\sigma_{NN} = \frac{N\gamma}{|\gamma-\chi|}, \tag{24}$$

which is shot-noise-limited at $\chi = 0$ (i.e., at no internal squeezing), but can be made to surpass it for $\chi > 0$. We have therefore recovered the internal squeezing approach to enhancing the quantum-limited sensitivity previously developed in [20–22].

In Appendix C we demonstrate this approach starting with a second-order transfer function, arriving again at an internal squeezing design, with the same condition $\gamma = \chi$ resulting in a divergent response.

VI. REALIZATION OF QND VIA SIGNAL AMPLIFICATION

In this section we consider the nonminimal realization of a passive first-order transfer function, showing that the shot-noise limit can be surpassed for a classical signal coupled linearly to one of the modes via the addition of hidden internal modes that internally amplify the signal. We again choose the classical signal to be a displacement of the cavity length, as discussed in Sec. III, although the analysis remains general to all linear detectors. We first show

that the minimal realization of a first-order system without squeezing is constrained by the Mizuno limit [42], and use the recent discovery that an infinite dc signal response can be achieved by adding a pair of modes that do not manifest in the input-output dynamics [23] and thus do not add any additional noise. We show how this is the simplest case of a general class of such nonminimal realizations, and that a quantum-mechanics-free subspace is formed, allowing for arbitrary modification of the system dynamics. By asserting that the input-output behavior remains the same, we have internal signal amplification without adding additional noise channels.

First, considering the case of Eq. (16) without squeezing with $\alpha = \beta \equiv \gamma$, the physically realizable state space is given by

$$\mathbf{G}^q(\Omega) = \begin{bmatrix} \dfrac{\Omega - i\gamma}{\Omega + i\gamma} & 0 \\ 0 & \dfrac{\Omega - i\gamma}{\Omega + i\gamma} \end{bmatrix}. \tag{25}$$

The corresponding generalized open oscillator is given by

$$S = I_{2\times 2}, \quad \hat{L} = -\sqrt{2\gamma}\hat{a}, \quad \hat{H} = 0, \tag{26}$$

and the corresponding minimal realization is a simple tuned cavity where γ is the cavity bandwidth. We can express the dynamics in the sideband picture by the Langevin equation and associated input-output relation [41,43–45]

$$\dot{\hat{a}} = -\gamma\hat{a} + \sqrt{2\gamma}\hat{a}_{\text{in}}, \tag{27}$$

$$\hat{a}_{\text{out}} = \hat{a}_{\text{in}} - \sqrt{2\gamma}\hat{a}. \tag{28}$$

As before, we choose the classical signal x_c to be the length modulation of the $\hat{a}$ cavity, which is coupled linearly to the amplitude quadrature of the cavity, and therefore apply the aforementioned linearization process to the radiation pressure coupling. The transfer function from the input vacuum to the amplitude quadrature is given by

$$G_{uF}(\Omega) = \frac{\sqrt{2\gamma}}{\gamma - i\Omega}. \tag{29}$$

Integrating this over all frequencies gives 2π and thus the total SNR will be bounded by a constant independent of the bandwidth. This fact is the aforementioned Mizuno limit. Specifically, the detector is limited by the shot-noise limit $\sigma_{NN} = N$ where N is the average photon number, giving $\text{SNR} = \omega_0^2 N^2/2 = E^2/(2\hbar^2)$ where E is the average energy. Passive resonant detectors generally exhibit such a limit: dependent on the average stored energy, but independent of the parameters.

We now consider adding two auxiliary modes $\hat{b}$ and $\hat{c}$ as shown in Fig. 2 and discussed in [23], without modifying the input-output dynamics. In Appendix D we derive a general approach by which such hidden auxiliary modes can be added. The general condition is given by

$$T^{(a)}(\Omega) \equiv \begin{bmatrix} ig_b & -ig_{b^\dagger} \\ ig_{b^\dagger}^* & -ig_b^* \end{bmatrix} T^{(b)}(\Omega) + \begin{bmatrix} ig_c & -ig_{c^\dagger} \\ ig_{c^\dagger}^* & -ig_c^* \end{bmatrix} T^{(c)}(\Omega) = 0. \tag{30}$$

where $T^{(b)}(\Omega)$ and $T^{(c)}(\Omega)$ are transfer functions given in Eqs. (D15) and (D16) respectively, and the most general linear Hamiltonian with two extra possibly hidden modes is given by

$$-\hbar g_b(\hat{a}\hat{b}^\dagger + \hat{a}^\dagger\hat{b}) - \hbar g_{b^\dagger}(\hat{a}\hat{b} + \hat{a}^\dagger\hat{b}^\dagger),$$
$$-\hbar g_c(\hat{a}\hat{c}^\dagger + \hat{a}^\dagger\hat{c}) - \hbar g_{c^\dagger}(\hat{a}\hat{c} + \hat{a}^\dagger\hat{c}^\dagger).$$

The terms with coupling rates g_b and g_c are coupled to $\hat{a}$ via a beam splitter, and the terms with coupling rates $g_{b^\dagger}$ and $g_{c^\dagger}$ via a nonlinear crystal (or equivalently an optomechanical interaction with optomechanical coupling frequency g, as discussed in [15,23]). Each auxiliary mode has just one degree of freedom, and thus the transfer functions are given by

$$T^{(b)}(\Omega) = \frac{1}{-i\Omega}\begin{bmatrix} ig_b & -ig_{b^\dagger} \\ ig_{b^\dagger}^* & -ig_b^* \end{bmatrix}, \tag{31}$$

$$T^{(c)}(\Omega) = \frac{1}{-i\Omega}\begin{bmatrix} ig_c & -ig_{c^\dagger} \\ ig_{c^\dagger}^* & -ig_c^* \end{bmatrix}. \tag{32}$$

This gives

$$T^{(a)}(\Omega) \equiv \frac{1}{-i\Omega}(-g_b^2 + g_{b^\dagger}^2 - g_c^2 + g_{c^\dagger}^2)I_{2\times 2}. \tag{33}$$

If we now choose cavity mode $\hat{c}$ to be coupled to mode $\hat{a}$ purely by a beam splitterlike interaction, then we have $g_c = \omega_s$ with ω_s being the sloshing frequency between the mode $\hat{c}$ and mode $\hat{a}$ and no nonlinear coupling: $g_{c^\dagger} = 0$. Therefore the input-output dynamics is left invariant if $g_b = 0$ and $g_{b^\dagger} = \omega_s$, and so mode $\hat{b}$ should be coupled to mode $\hat{a}$ via a nonlinear interaction (e.g., a nonlinear crystal if $\hat{b}$ is an optical mode) with the same coupling constant as the $\hat{c}$ mode: $g \equiv g_{b^\dagger} = \omega_s$. The most general Hamiltonian with two hidden modes is thus given by

$$\hat{H}_0 = -\hbar g(\hat{a}\hat{c}^\dagger + \hat{a}^\dagger\hat{c}) - \hbar g(\hat{a}\hat{b} + \hat{a}^\dagger\hat{b}^\dagger). \tag{34}$$

Such a system is known as being parity-time symmetric (PT symmetric) as the Hamiltonian is invariant under the parity operation (reversing modes $\hat{c}$ and $\hat{b}$ via $\hat{c} \leftrightarrow \hat{b}^\dagger$,

$\hat{c}^\dagger \leftrightarrow \hat{b}$) together with the time-reversal operation ($\hat{c} \leftrightarrow \hat{c}^\dagger$, $\hat{b} \leftrightarrow \hat{b}^\dagger$) [46]. The equations of motion are given by

$$\dot{\hat{a}} = -\gamma\hat{a} + ig\hat{c} + ig\hat{b}^\dagger + \sqrt{2\gamma}\hat{a}_{\rm in}, \tag{35}$$

$$\dot{\hat{b}}^\dagger = -ig\hat{a}, \tag{36}$$

$$\dot{\hat{c}} = ig\hat{a}. \tag{37}$$

In this case, we have the probe degree of freedom proportional to the amplitude quadrature of the $\hat{c}$ mode cavity $\hat{F} \propto (\hat{c} + \hat{c}^\dagger)/\sqrt{2}$ and the input as the amplitude quadrature $\hat{u} = (\hat{a}_{\rm in} + \hat{a}_{\rm in}^\dagger)/\sqrt{2}$. Solving in the frequency domain, we can find the input-to-probe transfer function

$$G_{uF}(\Omega) \propto \frac{g}{\Omega}\frac{\sqrt{2\gamma}}{\gamma - i\Omega}, \tag{38}$$

and therefore the probe fluctuation S_{FF} diverges at dc and thus σ_{NN} diverges and the detector is optimized in the regime where the photon number fluctuation is less than the mean. In this case we are not necessarily operating at or above threshold and thus the pump depletion approximation mentioned in the internal squeezing case is not relevant here.

We can show that the diverging probe fluctuation occurs due to the setup realizing an ideal QND measurement [26], in which case the probe degree of freedom has infinite fluctuation as it is conjugate to a conserved QND quantity.

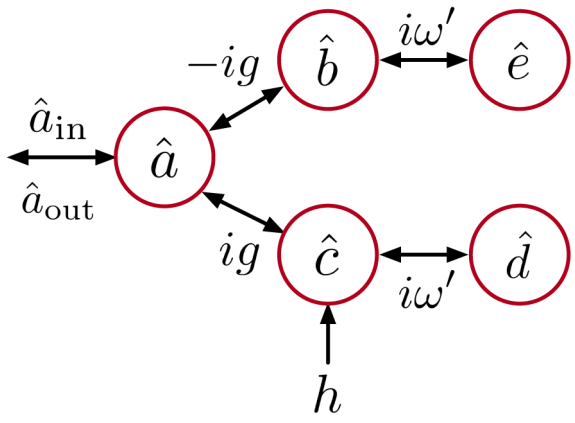

FIG. 2. A schematic representation of the most complex realization developed in Sec. VI. The modes $\hat{b}$ and $\hat{c}$ are coupled to the mode $\hat{a}$ via a squeezinglike interaction and beam splitterlike interaction respectively with the same coupling frequency g, with the signal h being coupled to mode $\hat{c}$. In this setup the signal response diverges at dc. We then add two additional modes $\hat{d}$ and $\hat{e}$ coupled to the modes $\hat{b}$ and $\hat{c}$ respectively, both via beam splitterlike couplings with coupling frequency ω' which shifts the signal response resonance to $\Omega = \omega'$.

Rewriting Eq. (34),

$$\hat{H}_0 = -\hbar g[\hat{a}^\dagger(\hat{c} + \hat{b}^\dagger) + \hat{a}(\hat{c}^\dagger + \hat{b})], \tag{39}$$

it can be seen that the composite quantity $\hat{c} + \hat{b}^\dagger$ is conserved, since

$$\frac{d}{dt}(\hat{c} + \hat{b}^\dagger) \propto [\hat{c} + \hat{b}^\dagger, \hat{c}^\dagger + \hat{b}] = 0. \tag{40}$$

This further implies two conserved quantities $\hat{X}_+ \equiv (\hat{X}_c + \hat{X}_b)/\sqrt{2}$, $\hat{Y}_- \equiv (\hat{Y}_c - \hat{Y}_b)/\sqrt{2}$ in terms of amplitude and phase quadratures $\hat{X}_c \equiv (\hat{c} + \hat{c}^\dagger)/\sqrt{2}$, $\hat{Y}_c \equiv (\hat{c} - \hat{c}^\dagger)/\sqrt{2}i$ (and similarly for $\hat{a}$ and $\hat{b}$). Additionally, we define $\hat{X}_- \equiv (\hat{X}_c - \hat{X}_b)/\sqrt{2}$. Rewriting the Hamiltonian in terms of these quantities gives

$$\hat{H}_0 = \hbar g(\hat{Y}_a\hat{X}_+ - \hat{X}_b\hat{Y}_-) - \hbar(\alpha/\sqrt{2})(\hat{X}_+ + \hat{X}_-)h, \tag{41}$$

The relevant residue part leading to detection of the signal x_c reads

$$\hat{H}_{\rm res} = -\hbar g\hat{X}_a\hat{Y}_- - \hbar(\alpha/\sqrt{2})\hat{X}_- x_c, \tag{42}$$

with $\hat{Y}_-$ being the conserved QND observable and $\hat{X}_-$ being the probe degree of freedom thus having infinite variance and therefore giving infinite signal response. In the frequency domain, $\hat{Y}_-$ exhibits the divergence at dc:

$$\hat{Y}_-(\Omega) = \frac{i\alpha}{\sqrt{2}\Omega}x_c(\Omega). \tag{43}$$

As discovered above, the operators $\hat{X}_+$ and $\hat{Y}_-$ are constants of motion and therefore form a quantum-mechanics-free subsystem ([28, §III],[29, Appendix D], [30,31]). The dynamics can be arbitrarily modified while keeping this subsystem quantum-mechanics-free so long as the simultaneous measurability condition is kept:

$$[\hat{X}_+(t), \hat{X}_+(t')] = [\hat{Y}_-(t), \hat{Y}_-(t')] = 0. \tag{44}$$

We can then modify the dynamics such that the signal response appears to diverge under the approximations of our analysis. As an example, we can shift the divergent response from dc to another frequency ω' by adding an extra pair of modes $\hat{d}$ and $\hat{e}$ which couple to $\hat{b}$ and $\hat{c}$, respectively. In this case the interaction Hamiltonian gains the terms

$$\begin{aligned}&-\hbar\omega'(\hat{b}\hat{d}^\dagger + \hat{b}^\dagger\hat{d} + \hat{c}^\dagger\hat{e} + \hat{c}\hat{e}^\dagger)\\ &\quad = i\hbar\omega'(\hat{X}_+\hat{Q}_+ + \hat{Y}_+\hat{P}_+ - \hat{Y}_-\hat{P}_- + \hat{X}_-\hat{Q}_-),\end{aligned}$$

which satisfies the general condition given in Eq. (30) and thus does not affect the input-output dynamics, and where

we have defined

$$\hat{Q}_{\pm} \equiv \frac{\hat{X}_d \pm \hat{X}_e}{\sqrt{2}}, \quad \hat{P}_{\pm} \equiv \frac{\hat{Y}_d \pm \hat{Y}_e}{\sqrt{2}}. \tag{45}$$

The residue part relevant to signal detection gains the term

$$\hbar\omega'(\hat{X}_-\hat{Q}_- - \hat{Y}_-\hat{P}_-). \tag{46}$$

The latter term modifies the dynamics of $\hat{Y}_-$ to become

$$\dot{\hat{Y}}_- = -\omega'\hat{Q}_- + \frac{\alpha}{\sqrt{2}}x_c, \tag{47}$$

$$\dot{\hat{Q}}_- = \omega'\hat{Y}_-, \tag{48}$$

and so, eliminating $\hat{Q}_-$ in the frequency domain, we obtain

$$\hat{Y}_-(\Omega) = \frac{i\alpha\Omega}{\sqrt{2}(\Omega^2 - \omega'^2)}x_c(\Omega). \tag{49}$$

We see that the signal response now diverges at $\Omega = \omega'$ rather than at dc, and that the *PT*-symmetric case shown in Eq. (43) is recovered for $\omega' = 0$. The final- phase quadrature input-output relation is given by

$$\hat{Y}_{\text{out}}(\Omega) = -\frac{\Omega - i\gamma}{\Omega + i\gamma}\hat{Y}_{\text{in}}(\Omega) + \frac{\sqrt{\gamma}\alpha g\Omega x_c(\Omega)}{(\Omega^2 - \omega'^2)(\Omega + i\gamma)}, \tag{50}$$

and so via the divergent signal amplification we now have an infinite signal response at a chosen frequency.

VII. DISCUSSION

We have demonstrated a systematic method for constructing detectors that are optimal up to the approximation that the photon number fluctuation approaches the mean, specifically investigating the first-order transfer function. Investigating minimal realizations of the transfer function, we showed that the optimal designs use internal squeezing. Considering nonminimal realizations, we investigated *PT*-symmetric systems and showed that such systems realize a QND measurement and are optimal, further showing how their dynamics can be modified without losing this property.

Another further exploration will be a systematic realization of the transmission-readout setup presented in [15]; however, this requires systematically realizing a 4×4 multi-input, multi-output (MIMO) transfer function with third-order elements, which will be complicated to realize directly using the aforementioned framework. Further, we can consider experimental demonstrations of the aforementioned *PT*-symmetric setups. Optomechanical realizations are currently in development; however, there is also the open possibility for an all-optical demonstration that avoids the strict thermal noise requirements expected in the optomechanical design. Finally, the aforementioned signal amplification readout is less susceptible to output loss at the photodiode than the internal squeezing setup due to the amplification of the signal, so different realizations have different responses to loss and thus we can choose the specific realization to minimize the impact of loss on the SNR. One future approach would be a full analysis taking loss into account from the start by adding the additional loss channels to a MIMO transfer function, fixing the loss coefficient to be small, and then using the framework to systematically realize this transfer function.

ACKNOWLEDGMENTS

We would like to thank Denis Martynov, LIGO AIC, and QNWG for fruitful discussions. J.B. is supported by the STFC and School of Physics and Astronomy at the University of Birmingham. J.B. and H.M. acknowledge the additional support from the Birmingham Institute for Gravitational Wave Astronomy. H.M. has also been supported by UK STFC Ernest Rutherford Fellowship (Grant No. ST/M005844/11). Y.C. is supported by the Simons Foundation (Award No. 568762), and the National Science Foundation, through Grants No. PHY-1708212 and No. PHY-1708213.

APPENDIX A: LINEAR SYSTEMS

The general solution for $\mathbf{x}$ and $\mathbf{y}$ of the linear system (1) is

$$\mathbf{x}(t) = e^{At}\mathbf{x}(0-) + \int_{0-}^{t} e^{A(t-\tau)}B\mathbf{u}(\tau)d\tau,$$

$$\mathbf{y}(t) = \mathrm{C}e^{At}\mathbf{x}(0-) + \int_{0-}^{t} \mathrm{C}e^{A(t-\tau)}B\mathbf{u}(\tau)d\tau + D\mathbf{u}(t).$$

Taking the initial condition to be at $t = 0^-$ allows the consideration of impulse inputs $\delta(t)$ and a step discontinuity in $\mathbf{x}$ from $t = 0^-$ to $t = 0^+$ (the time just after $t = 0$).

The system is asymptotically stable if the matrix A is Hurwitz, that is, all its eigenvalues have a negative real part. In an asymptotically stable system, the natural response asymptotically decays to zero, $\lim_{t\to\infty} e^{At}\mathbf{x}(0^-) = 0$ for any initial condition $\mathbf{x}(0^-)$. The impulse response h for an asymptotically stable system also decays to 0 as $t \to \infty$.

For a sinusoid input $\mathbf{u}(t) = \mathbf{b}(\Omega)e^{-i\Omega t}$, where Ω is real and $\mathbf{b}(\Omega)$ is a fixed column vector of operators (in our case this vector contains the quantized modes of an input quantum field), the asymptotic output as $t \to \infty$ of an asymptotically stable system only has the forced response

and is given by

$$\mathbf{y}(t) = H(\Omega)\mathbf{b}(\Omega)e^{-i\Omega t}, \tag{A1}$$

where $H(\Omega)$ is as given in (2) with $\sigma \geq 0$. In this case, H coincides with the Fourier transform of h and is called the system's frequency response. For an input $\mathbf{u}(t) = \int_{-\infty}^{\infty} \mathbf{b}(\Omega)e^{-i\Omega t}d\Omega$, by linearity of the system the asymptotic response is $\mathbf{y}(t) = \int_{-\infty}^{\infty} H(\Omega)\mathbf{b}(\Omega)e^{-i\Omega t}d\Omega$.

For a system that is not asymptotically stable, the impulse response may not be integrable, $\int_{0^-}^{\infty} |h(t)|dt = \infty$, and the frequency response H not well defined. For such systems, the forced response to a sinusoid input may not have an asymptotic solution. However, for $h(t) = O(e^{\sigma t})$, with $\sigma \geq 0$, it can have an asymptotic solution for inputs of the form $\mathbf{u}(t) = \mathbf{b}(\Omega)e^{-i\Omega t}$ for all complex Ω with $\mathrm{Im}\{\Omega\} > \sigma$ and with $\mathbf{b}(\Omega)$ some fixed vector of operators as before. In this case, the asymptotic forced response is again given by the right-hand side of (A1) but Ω is now complex. For more general inputs of the form $\mathbf{u}(t) = \int_{-\infty}^{\infty} \mathbf{b}(\omega + i\sigma_0)e^{-i(\omega+i\sigma_0)t}d\omega$, with $\sigma_0 > \sigma$, by linearity the forced response is given by $\mathbf{y}_f(t) = \int_{-\infty}^{\infty} H(\omega + i\sigma_0)\mathbf{b}(\omega + i\sigma_0)e^{-i(\omega+i\sigma_0)t}d\omega$.

APPENDIX B: PHYSICALLY REALIZABLE STATE-SPACE REALIZATION FOR INTERNAL SQUEEZING

We will now follow the steps given in [25] to systematically construct the physically realizable state space of the internal squeezing setup whose transfer function is shown in Eq. (16). First we define a de-dimensionalized frequency with respect to α by making the transformation $\Omega \to \alpha\Omega$, so that the aforementioned transfer function becomes

$$\mathbf{G}^q(\Omega) = \begin{bmatrix} \dfrac{1+i\Omega}{\Gamma - i\Omega} & 0 \\ 0 & \dfrac{\Gamma + i\Omega}{1 - i\Omega} \end{bmatrix}, \tag{B1}$$

where $\Gamma \equiv \beta/\alpha$. The recovery of a linear quantum system (1) with $\mathbf{G}^q(\Omega)$ as its transfer function is studied in modern control theory as a fundamental topic known as realization theory; see, for example, [47] for a review. We do not describe the calculations for finding a state-space realization for the transfer function given above, but we describe below how it may can computed with Mathematica routines.

Assuming that the amplitude quadrature is squeezed (i.e., $\Gamma < 1$), we can compute the canonical state-space realization using Mathematica. The Mathematica function `StateSpaceModel` when applied to a transfer function returns a state space in the controllable canonical form [48,49]. The returned state space may have more internal degrees of freedom than is necessary to represent the system. This is remedied by applying the function `MinimalStateSpaceModel` [50] to the state space to find the minimal state space [51]. Using these functions, we calculate

$$A' = \frac{1}{3+\gamma^2}\begin{bmatrix} -(1+\Gamma)^2 & c_1 \\ c_1 & -2-\Gamma-\Gamma^3 \end{bmatrix}, \tag{B2}$$

$$B' = \begin{bmatrix} 0 & \sqrt{\dfrac{2}{3+\Gamma^2}} \\ \dfrac{1}{2}\sqrt{\dfrac{3+\Gamma^2}{1+\Gamma^2}} & \dfrac{\Gamma^2-1}{2\sqrt{3+4\Gamma^2+\Gamma^4}} \end{bmatrix}, \tag{B3}$$

$$C' = \begin{bmatrix} \dfrac{(1+\Gamma)^2|\Gamma-1|}{\sqrt{2(3+\Gamma^2)}} & \dfrac{2(1+\Gamma)(1+\Gamma^2)}{\sqrt{3+4\Gamma^2+\Gamma^4}} \\ (1+\Gamma)\sqrt{\dfrac{3+\Gamma^2}{2}} & 0 \end{bmatrix}, \tag{B4}$$

$$D' = -I_{2\times 2}. \tag{B5}$$

where $c_1 = \sqrt{2}\sqrt{1+\Gamma^2}|\Gamma - 1|$ and $I_{2\times 2}$ is the 2×2 identity matrix. This state space does not currently fulfill the physical realizability condition, given by [25]

$$AJ + JA^\dagger + BJB^\dagger = 0, \tag{B6}$$

$$JC^\dagger + BJD^\dagger = 0, \tag{B7}$$

where

$$J = \begin{bmatrix} 1 & 0 \\ 0 & -1 \end{bmatrix}. \tag{B8}$$

To find the transformation from the unrealizable state space (A', B', C', D') to the realizable state space (A, B, C, D) we look for the matrix X that satisfies

$$A'X + X(A')^\dagger + B'J(B')^\dagger = 0, \tag{B9}$$

$$X(C')^\dagger + B'J(D')^\dagger = 0. \tag{B10}$$

In this case one such matrix is given by

$$X = \begin{bmatrix} -\dfrac{2}{3+3\Gamma+\Gamma^2+\Gamma^3} & \dfrac{\sqrt{3+4\Gamma^2+\Gamma^4}|\Gamma-1|}{\sqrt{2}(1+\Gamma^2)(3+\Gamma^2)^{3/2}} \\ \dfrac{1-\Gamma}{\sqrt{2(1+\Gamma^2)}(3+\Gamma^2)} & \dfrac{2}{3+3\Gamma+\Gamma^2+\Gamma^3} \end{bmatrix}. \tag{B11}$$

We then look for the similarity transformation matrix T satisfying $X = TJT^\dagger$, which in this case is given by

$$T = \begin{bmatrix} 0 & \sqrt{\dfrac{2}{3+3\Gamma+\Gamma^2+\Gamma^3}} \\ \dfrac{1}{2}\sqrt{\dfrac{3+\Gamma^2}{1+\Gamma+\Gamma^2+\Gamma^3}} & \dfrac{\Gamma^2-1}{2\sqrt{(1+\Gamma^2)(3+3\Gamma+\Gamma^2+\Gamma^3)}} \end{bmatrix}. \tag{B12}$$

We can apply this transformation by the standard state-space transformation,

$$A = T^{-1}A'T, \quad B = T^{-1}B', \quad C = C'T, \quad D = D', \tag{B13}$$

which gives the state space

$$A = \frac{1}{2}\begin{bmatrix} -1-\Gamma & 1-\Gamma \\ |-1+\Gamma| & -1-\Gamma \end{bmatrix}, \tag{B14}$$

$$B = \sqrt{1+\Gamma}I_{2\times 2}, \tag{B15}$$

$$C = \sqrt{1+\Gamma}I_{2\times 2}, \tag{B16}$$

$$D = -I_{2\times 2}. \tag{B17}$$

To slightly simplify the physical realization without loss of generality we can add a π phase shift for the input-output reflection, resulting in transforming the state space via $C \to -C$ and $D \to -D$. Substituting $\Gamma = \beta/\alpha$ and reversing the de-dimensionalization via $\Omega \to \Omega/\alpha$, we obtain the physically realizable state space which obeys Eqs. (B6) and (B7),

$$A = \frac{1}{2}\begin{bmatrix} -\alpha-\beta & \alpha-\beta \\ \alpha-\beta & -\alpha-\beta \end{bmatrix},$$
$$B = \sqrt{\alpha+\beta}\, I_{2\times 2}, \tag{B18}$$
$$C = -\sqrt{\alpha+\beta}\, I_{2\times 2}, D = I_{2\times 2}.$$

APPENDIX C: QUANTUM EXPANDER

In this appendix we consider a second-order input-output transfer function, showing that the optimal sensitivity is achieved when the parameters match that of the so-called quantum expander explored in [22], a setup which, similarly to the transmission-readout setup discussed in [15], can directly increase the detection bandwidth of a gravitational wave interferometer. This setup, shown in Fig. 3, consists of a tuned, signal-recycled Michelson interferometer with internal squeezing in the signal recycling cavity. The signal-recycled Michelson can be mapped to an equivalent coupled-cavity [52]. We show that the quantum expander is the optimal detector for any second-order quadrature-picture transfer function obeying the constraints in Sec. IV.

Thus we start with the most general rational and proper second-order input-output transfer function that is diagonal and rational,

$$\mathbf{G}^q(\Omega) = \begin{bmatrix} \dfrac{(i\Omega-\alpha_1)(i\Omega-\beta_1)}{(i\Omega-\alpha_2)(i\Omega-\beta_2)} & 0 \\ 0 & \dfrac{(-i\Omega-\alpha_2)(-i\Omega-\beta_2)}{(-i\Omega-\alpha_1)(-i\Omega-\beta_1)} \end{bmatrix}, \tag{C1}$$

where $\alpha_1, \alpha_2, \beta_1, \beta_2 \in \mathbb{R}$. Requiring that there is no gain at dc, we also obtain the condition $\alpha_1\beta_1 = \alpha_2\beta_2$. We then follow the same procedure as in Appendix B for finding the physically realizable state space, obtaining

$$A = \begin{bmatrix} 0 & 0 & -i\omega_s & 0 \\ 0 & 0 & 0 & i\omega_s \\ -i\omega_s & 0 & -\gamma & -\chi \\ 0 & i\omega_s & -\chi & -\gamma \end{bmatrix},$$

$$B = \begin{bmatrix} 0 & 0 \\ 0 & 0 \\ \sqrt{2}\sqrt{\gamma} & 0 \\ 0 & \sqrt{2}\sqrt{\gamma} \end{bmatrix},$$

$$C = \begin{bmatrix} 0 & 0 & -\sqrt{2}\sqrt{\gamma} & 0 \\ 0 & 0 & 0 & -\sqrt{2}\sqrt{\gamma} \end{bmatrix}, \quad D = I_{2\times 2}, \tag{C2}$$

where $\gamma \equiv \frac{1}{2}(-\alpha_1+\alpha_2-\beta_1+\beta_2)$, $\chi \equiv \frac{1}{2}(\alpha_1+\alpha_2\beta_1+\beta_2)$, and $\omega_s \equiv \sqrt{\alpha_1\beta_1}$. This corresponds to the dynamics derived from Hamiltonian for the quantum expander

described in [22]. In this case since we have a two-degree-of-freedom system, we have to apply the separation theorem of [32] to separate it into two one-degree-of-freedom systems. The corresponding quantum network is given by $\mathcal{N} = \{\{G_1, G_2\}, \hat{H}^d, \mathcal{S}\}$, where $\mathcal{S} = G_2 \triangleleft G_1$ represents the series product [29], that is, the output of G_1 is fed into G_2. The two generalized open oscillators are given by

$$G_1 = (I_{2\times 2}, 0, 0)\,, \tag{C3}$$

$$G_2 = \left(I_{2\times 2}, -\sqrt{2\gamma}\hat{a}_q, \tfrac{i}{2}\hbar\chi(\hat{a}_q\hat{a}_q + \hat{a}_q^\dagger\hat{a}_q^\dagger)\right), \tag{C4}$$

where $I_{2\times 2}$ is the 2×2 identity matrix, γ is the coupling frequency of the continuum to the cavity mode described by annihilation operator $\hat{a}_q$, and χ is the strength of the nonlinear interaction. The Hamiltonian coupling the two cavities is given by $\hat{H}^d = \hbar\omega_s(\hat{a}_q\hat{a}^\dagger + \hat{a}_q^\dagger\hat{a})$, where $\hat{a}$ is the cavity mode of the second cavity, and is therefore a simple beam splitterlike coupling between the two cavities. Note that G_1 is not coupled to the external continuum and therefore it is only coupled to G_2 via H^d. In total we have two tuned cavities coupled by a beam splitter-like interaction, with the first cavity coupled to the external continuum and exhibiting internal squeezing, and have thus recovered the quantum expander realization pictured in Fig. 3.

The quadrature transfer function from the input to the arm cavity mode $\hat{a}$ was found to be

$$\begin{bmatrix}\hat{a}^1\\ \hat{a}^2\end{bmatrix} = \begin{bmatrix} 0 & \dfrac{\sqrt{2\gamma}\omega_s}{i\omega(\chi-\gamma)+\omega_s^2-\omega^2}\\ -\dfrac{\sqrt{2\gamma}\omega_s}{-i\omega(\gamma+\chi)+\omega_s^2-\omega^2} & 0\end{bmatrix}\begin{bmatrix}\hat{a}_{\rm in}^1\\ \hat{a}_{\rm in}^2\end{bmatrix}. \tag{C5}$$

Using Eq. (7), we see that the SNR for a signal coupled to the amplitude quadrature is given by $2\pi\gamma/|\gamma-\chi|$, which diverges as $\chi\to\gamma$. At $\chi\gg\gamma$ the SNR approaches zero since the nonlinear interaction totally depletes the amplitude quadrature fluctuations in the cavity. The SNR for the phase quadrature is given by $2\pi\gamma/(\gamma+\chi)$, which is maximal at $\chi = 0$ where it is equal to 2π and is thus constrained by the Mizuno limit.

For the signal recycling cavity mode $\hat{a}_q$, we also see the divergence at $\chi\to\gamma$, except that in this case the SNR for the phase quadrature diverges rather than the amplitude quadrature,

$$\begin{bmatrix}\hat{a}_q^1\\ \hat{a}_q^2\end{bmatrix} = \begin{bmatrix} -\dfrac{i\sqrt{2}\sqrt{\gamma}\omega}{-i\omega(\gamma+\chi)+\omega_s^2-\omega^2} & 0\\ 0 & -\dfrac{i\sqrt{2}\sqrt{\gamma}\omega}{i\omega(\chi-\gamma)+\omega_s^2-\omega^2}\end{bmatrix}\begin{bmatrix}\hat{a}_{\rm in}^1\\ \hat{a}_{\rm in}^2\end{bmatrix}. \tag{C6}$$

In this case the SNR for the amplitude quadrature is given by $2\pi\gamma/(\gamma+\chi)$ and for the phase quadrature is given by $2\pi\gamma/|\gamma-\chi|$, that is, the roles of the amplitude and phase quadrature are swapped compared to the arm-cavity mode.

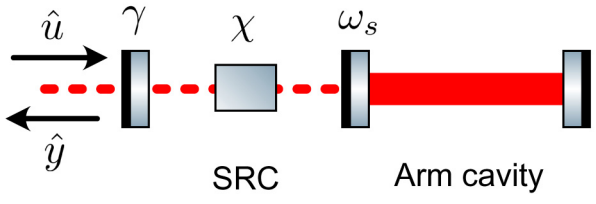

FIG. 3. The setup analyzed for the quantum expander as explored in [22], equivalent to a tuned Michelson interferometer except with squeezing (via a nonlinear crystal) internally within the signal recycling cavity (SRC).

APPENDIX D: AUXILIARY MODE DYNAMICS

In this section we discuss how the dynamics of added auxiliary modes, shown in Fig. 2, can be inferred by requiring that the frequency-domain input-output relation remain unchanged by the addition of them. Each auxiliary mode is coupled to a set of n_d internal modes $\hat{d}_j$ and n_e internal

modes $\hat{e}_j$, adding the following terms to the Hamiltonian:

$$\begin{aligned}
&\sum_j -\hbar g_{d_j}(\hat{b}\hat{d}_j^\dagger + \hat{b}^\dagger \hat{d}_j) - \hbar g_{d_j^\dagger}(\hat{b}\hat{d}_j + \hat{b}^\dagger \hat{d}_j^\dagger) \\
&\quad - \hbar g_{e_j}(\hat{c}\hat{e}_j^\dagger + \hat{c}^\dagger \hat{e}_j) - \hbar g_{e_j^\dagger}(\hat{c}\hat{e}_j + \hat{c}^\dagger \hat{e}_j^\dagger) \\
&\quad + \sum_{i\neq j} \hbar g_{d_i d_j^\dagger}(\hat{d}_i \hat{d}_j^\dagger + \hat{d}_i^\dagger \hat{d}_j) + \hbar g_{d_i d_j}(\hat{d}_i \hat{d}_j + \hat{d}_i^\dagger \hat{d}_j^\dagger) \\
&\quad + \sum_{i\neq j} \hbar g_{e_i e_j^\dagger}(\hat{e}_i \hat{e}_j^\dagger + \hat{e}_i^\dagger \hat{e}_j) + \hbar g_{e_i e_j}(\hat{e}_i \hat{e}_j + \hat{e}_i^\dagger \hat{e}_j^\dagger),
\end{aligned}$$

where $g_{d_i d_j^\dagger}$ and $g_{d_i d_j}$ respectively quantify the beam splitterlike and nonlinear coupling between modes $\hat{d}_i$ and $\hat{d}_j$, and similarly for the $\hat{e}$ modes. Note that there is no direct coupling between the $\hat{d}$ and $\hat{e}$ modes.

The full set of equations of motion is

$$\begin{aligned}
\dot{\hat{a}} &= -\gamma \hat{a} + \sqrt{2\gamma}\hat{a}_{\text{in}} \\
&\quad - i g_b \hat{b} + i g_{b^\dagger} \hat{b}^\dagger - i g_c \hat{c} + i g_{c^\dagger} \hat{c}^\dagger, && \text{(D1)} \\
\dot{\hat{b}} &= i g_b \hat{a} - i g_{b^\dagger} \hat{a}^\dagger + i \sum_j g_{d_j} \hat{d}_j - i \sum_j g_{d_j^\dagger} \hat{d}_j^\dagger, && \text{(D2)} \\
\dot{\hat{d}}_j &= i g_{d_j} \hat{b} + i g_{d_j^\dagger} \hat{b}^\dagger - i \sum_{i\neq j} g_{d_i d_j^\dagger} \hat{d}_i - i \sum_{i\neq j} g_{d_i d_j} \hat{d}_i^\dagger, && \text{(D3)} \\
\dot{\hat{c}} &= i g_c \hat{a} - i g_{c^\dagger} \hat{a}^\dagger + i \sum_j g_{e_j} \hat{e}_j - i \sum_j g_{e_j^\dagger} \hat{e}_j^\dagger, && \text{(D4)} \\
\dot{\hat{e}}_j &= i g_{e_j} \hat{c} + i g_{e_j^\dagger} \hat{c}^\dagger - i \sum_{i\neq j} g_{e_i e_j^\dagger} \hat{e}_i - i \sum_{i\neq j} g_{e_i e_j} \hat{e}_i^\dagger. && \text{(D5)}
\end{aligned}$$

Focusing on $\hat{d}_j$, the frequency-domain expression is given by

$$-i\Omega \vec{d}(\Omega) = \vec{g}_d \hat{b}(\Omega) + \vec{g}_{d^\dagger} \hat{b}^\dagger(-\Omega) - iG\vec{d}(\Omega), \quad \text{(D6)}$$

where

$$\vec{g}_d = (i g_{d_1}, -i g_{d_1^\dagger}^*, \ldots, i g_{d_{n_d}}, -i g_{d_{n_d}^\dagger}^*)^T, \quad \text{(D7)}$$

$$\vec{g}_{d^\dagger} = (i g_{d_j^\dagger}, -i g_{d_j}^*, \ldots, i g_{d_{n_d}^\dagger}, -i g_{d_{n_d}}^*)^T, \quad \text{(D8)}$$

and

$$\vec{d}(\Omega) = (\hat{d}_1(\Omega), \ldots, \hat{d}_{n_d}(\Omega); \hat{d}_1^\dagger(-\Omega), \ldots, \hat{d}_{n_d}^\dagger(-\Omega))^T. \quad \text{(D9)}$$

and where, in block form,

$$G^{(d)} = \begin{bmatrix} G_1^{(d)} \\ \vdots \\ G_{n_d}^{(d)} \end{bmatrix} \in \mathbb{C}^{2n_d \times 2n_d}, \quad \text{(D10)}$$

where

$$G_j^{(d)} = \begin{bmatrix} g_{d_1 d_j^\dagger} & \cdots & g_{d_{n_d} d_j^\dagger}; & g_{d_1 d_j} & \cdots & g_{d_{n_d} d_j} \\ g_{d_1 d_j^\dagger}^* & \cdots & g_{d_{n_d} d_j^\dagger}^*; & g_{d_1 d_j}^* & \cdots & g_{d_{n_d} d_j}^* \end{bmatrix}, \quad \text{(D11)}$$

with $g_{d_j d_j} = g_{d_j d_j^\dagger} = 0$. Solving for $\vec{d}(\Omega)$ gives

$$\begin{aligned}
\vec{d}(\Omega) &= (-i\Omega I_{2n_d \times 2n_d} + iG^{(d)})^{-1} \begin{bmatrix} \vec{g}_d & \vec{g}_{d^\dagger} \end{bmatrix} \begin{bmatrix} \hat{b}(\Omega) \\ \hat{b}^\dagger(-\Omega) \end{bmatrix} \\
&\equiv M^{(d)} \begin{bmatrix} \hat{b}(\Omega) \\ \hat{b}^\dagger(-\Omega) \end{bmatrix},
\end{aligned}$$

where $I_{2n_d \times 2n_d}$ is the $2n_d \times 2n_d$ identity matrix, and $M^{(d)} \in \mathbb{C}^{2n_d \times 2}$.

The frequency-domain expression for $\hat{b}$ is given by

$$-i\Omega \begin{bmatrix} \hat{b}(\Omega) \\ \hat{b}^\dagger(-\Omega) \end{bmatrix} = \begin{bmatrix} i g_b & -i g_{b^\dagger} \\ i g_{b^\dagger}^* & -i g_b^* \end{bmatrix} \begin{bmatrix} \hat{a}(\Omega) \\ \hat{a}^\dagger(-\Omega) \end{bmatrix} + iD^{(d)} \vec{d}(\Omega), \quad \text{(D12)}$$

where

$$D^{(d)} = \begin{bmatrix} g_{d_1}, & \ldots, & g_{d_{n_d}}; & -g_{d_1^\dagger}, & \ldots, & -g_{d_{n_d}^\dagger} \\ g_{d_1^\dagger}^*, & \ldots, & g_{d_{n_d}^\dagger}^*; & -g_{d_1}^*, & \ldots, & -g_{d_{n_d}}^* \end{bmatrix}. \quad \text{(D13)}$$

Solving for the $\hat{b}$ mode, we get

$$\begin{bmatrix} \hat{b}(\Omega) \\ \hat{b}^\dagger(-\Omega) \end{bmatrix} = T^{(b)}(\Omega) \begin{bmatrix} \hat{a}(\Omega) \\ \hat{a}^\dagger(-\Omega) \end{bmatrix}, \quad \text{(D14)}$$

where

$$T^{(b)}(\Omega) \equiv (-i\Omega I_{2\times 2} - iD^{(d)} M^{(d)})^{-1} \begin{bmatrix} i g_b & -i g_{b^\dagger} \\ i g_{b^\dagger}^* & -i g_b^* \end{bmatrix}, \quad \text{(D15)}$$

in which $I_{2\times 2}$ is the 2×2 identity matrix.

Similarly, we have

$$\begin{bmatrix} \hat{c}(\Omega) \\ \hat{c}^\dagger(-\Omega) \end{bmatrix} = T^{(c)}(\Omega) \begin{bmatrix} \hat{a}(\Omega) \\ \hat{a}^\dagger(-\Omega) \end{bmatrix},$$

where

$$T^{(c)}(\Omega) \equiv (-i\Omega I_{2\times 2} - iD^{(e)} M^{(e)})^{-1} \begin{bmatrix} i g_c & -i g_{c^\dagger} \\ i g_{c^\dagger}^* & -i g_c^* \end{bmatrix} \quad \text{(D16)}$$

in which

$$D^{(e)} = \begin{bmatrix} g_{e_1}, & \ldots, & g_{e_{ne}}; & -g_{e_1^\dagger}, & \ldots, & -g_{e_{ne}^\dagger} \\ g^*_{e_1^\dagger}, & \ldots, & g^*_{e_{ne}^\dagger}; & -g^*_{e_1}, & \ldots, & -g^*_{e_{ne}} \end{bmatrix}, \tag{D17}$$

and

$$M^{(e)} = (-i\Omega I_{2n_e \times 2n_e} + iG^{(e)})^{-1}, \tag{D18}$$

where, in block form,

$$G^{(e)} = \begin{bmatrix} G_1^{(e)} \\ \vdots \\ G_{n_e}^{(e)} \end{bmatrix} \in \mathbb{C}^{2n_e \times 2n_e}, \tag{D19}$$

where

$$G_j^{(e)} = \begin{bmatrix} g_{e_1 e_j^\dagger} & \cdots & g_{e_{n_e} e_j^\dagger}; & g_{e_1 e_j} & \cdots & g_{e_{n_e} e_j} \\ g^*_{e_1 e_j^\dagger} & \cdots & g^*_{e_{n_e} e_j^\dagger}; & g^*_{e_1 e_j} & \cdots & g^*_{e_{n_e} e_j} \end{bmatrix}. \tag{D20}$$

The frequency domain expression for $\hat{a}$ is given by

$$\begin{aligned} -i\Omega \begin{bmatrix} \hat{a}(\Omega) \\ \hat{a}^\dagger(-\Omega) \end{bmatrix} &= \begin{bmatrix} ig_b & -ig_{b^\dagger} \\ ig^*_{b^\dagger} & -ig^*_b \end{bmatrix} \begin{bmatrix} \hat{b}(\Omega) \\ \hat{b}^\dagger(-\Omega) \end{bmatrix} \\ &\quad + \begin{bmatrix} ig_c & -ig_{c^\dagger} \\ ig^*_{c^\dagger} & -ig^*_c \end{bmatrix} \begin{bmatrix} \hat{c}(\Omega) \\ \hat{c}^\dagger(-\Omega) \end{bmatrix} + \ldots, \\ &= T^{(a)}(\Omega) \begin{bmatrix} \hat{a}(\Omega) \\ \hat{a}^\dagger(-\Omega) \end{bmatrix} + \ldots \end{aligned}$$

where ... are the damping and input vacuum terms from Eq. (27) and where

$$\begin{aligned} T^{(a)}(\Omega) \equiv &\begin{bmatrix} ig_b & -ig_{b^\dagger} \\ ig^*_{b^\dagger} & -ig^*_b \end{bmatrix} T^{(b)}(\Omega) \\ &+ \begin{bmatrix} ig_c & -ig_{c^\dagger} \\ ig^*_{c^\dagger} & -ig^*_c \end{bmatrix} T^{(c)}(\Omega) = 0. \end{aligned} \tag{D21}$$

Therefore to keep the input-output dynamics invariant, all elements of this matrix must be zero.

[1] LIGO Scientific Collaboration, Advanced LIGO, Class. Quantum Grav. **32**, 74001 (2015).

[2] F. Acernese, M. Agathos, K. Agatsuma, D. Aisa, N. Allemandou, A. Allocca, J. Amarni, P. Astone, G. Balestri, and G. Ballardin, *et al.*, Advanced Virgo: A second-generation interferometric gravitational wave detector, Class. Quantum Grav. **32**, 024001 (2015).

[3] J. S. Read, C. Markakis, M. Shibata, K. Uryu, J. D. E. Creighton, and J. L. Friedman, Measuring the neutron star equation of state with gravitational wave observations, Phys. Rev. D **79**, 124033 (2009).

[4] A. Bauswein and H. T. Janka, Measuring Neutron-Star Properties via Gravitational Waves from Neutron-Star Mergers, Phys. Rev. Lett. **108**, 011101 (2012).

[5] C. Helstrom, Minimum mean-squared error of estimates in quantum statistics, Phys. Lett. A **25**, 101 (1967).

[6] V. B. Braginsky, in *AIP Conference Proceedings*, Vol. 523 (AIP, 2000), p. 180.

[7] A. Holevo, *Probabilistic and Statistical Aspects of Quantum Theory* (Scuola Normale Superiore, Pisa, 2011), 2nd ed.

[8] M. Tsang, H. M. Wiseman, and C. M. Caves, Fundamental Quantum Limit to Waveform Estimation, Phys. Rev. Lett. **106**, 090401 (2011).

[9] H. Miao, R. X. Adhikari, Y. Ma, B. Pang, and Y. Chen, Towards the Fundamental Quantum Limit of Linear Measurements of Classical Signals, Phys. Rev. Lett. **119**, 050801 (2017).

[10] H. Miao, N. D. Smith, and M. Evans, Quantum Limit for Laser Interferometric Gravitational-Wave Detectors from Optical Dissipation, Phys. Rev. X **9**, 011053 (2019).

[11] M. Zwierz, C. A. Pérez-Delgado, and P. Kok, Ultimate limits to quantum metrology and the meaning of the Heisenberg limit, Phys. Rev. A **85**, 042112 (2012).

[12] G. S. Pati, M. Salit, K. Salit, and M. S. Shahriar, Demonstration of a Tunable-Bandwidth White-Light Interferometer Using Anomalous Dispersion in Atomic Vapor, Phys. Rev. Lett. **99**, 133601 (2007).

[13] H. N. Yum, J. Scheuer, M. Salit, P. R. Hemmer, and M. S. Shahriar, Demonstration of white light cavity effect using stimulated Brillouin scattering in a fiber loop, J. Lightwave Technol. **31**, 3865 (2013).

[14] H. Miao, Y. Ma, C. Zhao, and Y. Chen, Enhancing the Bandwidth of Gravitational-Wave Detectors with Unstable Optomechanical Filters, Phys. Rev. Lett. **115**, 211104 (2015).

[15] J. Bentley, P. Jones, D. Martynov, A. Freise, and H. Miao, Converting the signal-recycling cavity into an unstable optomechanical filter to enhance the detection bandwidth of gravitational-wave detectors, Phys. Rev. D **99**, 102001 (2019).

[16] S. Daryanoosh, S. Slussarenko, D. W. Berry, H. M. Wiseman, and G. J. Pryde, Experimental optical phase measurement approaching the exact Heisenberg limit, Nat. Commun. **9**, 1 (2018).

[17] D. V. Tsarev, S. M. Arakelian, Y. L. Chuang, R. K. Lee, and A. P. Alodjants, Quantum metrology beyond Heisenberg limit with entangled matter wave solitons, Opt. Express **26**, 19583 (2018).

[18] J. Huang, M. Zhuang, B. Lu, Y. Ke, and C. Lee, Achieving Heisenberg-limited metrology with spin cat states via interaction-based readout, Phys. Rev. A **98**, 012129 (2018).

[19] S. Zhou, M. Zhang, J. Preskill, and L. Jiang, Achieving the Heisenberg limit in quantum metrology using quantum error correction, Nat. Commun. **9**, 78 (2018).

[20] V. Peano, H. G. L. Schwefel, C. Marquardt, and F. Marquardt, Intracavity Squeezing Can Enhance Quantum-Limited Optomechanical Position Detection through Deamplification, Phys. Rev. Lett. **115**, 243603 (2015).

[21] M. Korobko, L. Kleybolte, S. Ast, H. Miao, Y. Chen, and R. Schnabel, Beating the Standard Sensitivity-Bandwidth Limit of Cavity-Enhanced Interferometers with Internal Squeezed-Light Generation, Phys. Rev. Lett. **118**, 143601 (2017).

[22] M. Korobko, Y. Ma, Y. Chen, and R. Schnabel, Quantum expander for gravitational-wave observatories, Light: Sci. Appl. **8**, 118 (2019).

[23] X. Li, M. Goryachev, Y. Ma, M. Tobar, C. Zhao, R. X. Adhikari, and Y. Chen, Broadband sensitivity improvement via coherent quantum feedback with PT-symmetry (2020), ArXiv:2012.00836.

[24] X. Li, J. Smetana, A. Ubhi, J. Bentley, Y. Chen, Y. Ma, H. Miao, and D. Martynov, Enhancing interferometer sensitivity without sacrificing bandwidth and stability: beyond single-mode and resolved-sideband approximation, In preparation (2021).

[25] J. Bentley, H. Nurdin, Y. Chen, and H. Miao, Direct approach to realizing quantum filters for high-precision measurements, Phys. Rev. A **103**, 013707 (2021).

[26] V. B. Braginsky and F. Khalilli, *Quantum Measurement* (Cambridge University Press, Cambridge, 1992).

[27] N. Yamamoto, Coherent versus Measurement Feedback: Linear Systems Theory for Quantum Information, Phys. Rev. X **4**, 041029 (2014).

[28] M. R. James, H. I. Nurdin, and I. R. Petersen, H^∞ control of linear quantum stochastic systems, IEEE T. Automat. Contr. **53**, 1787 (2008).

[29] J. Gough and M. R. James, The series product and its application to quantum feedforward and feedback networks, IEEE T. Automat. Contr. **54**, 2530 (2009).

[30] M. Tsang and C. M. Caves, Evading Quantum Mechanics: Engineering a Classical Subsystem within a Quantum Environment, Phys. Rev. X **2**, 031016 (2012).

[31] S. Wang, H. I. Nurdin, G. Zhang, and M. R. James, Quantum optical realization of classical linear stochastic systems, Automatica **49**, 3090 (2013).

[32] H. I. Nurdin, M. R. James, and A. C. Doherty, Network synthesis of linear dynamical quantum stochastic systems, SIAM J. Control Optim. **48**, 2686 (2009).

[33] H. I. Nurdin and N. Yamamoto, *Linear Dynamical Quantum Systems: Analysis, Synthesis, and Control* (Springer, Berlin, 2017).

[34] M. Hush, A. R. R. Carvalho, M. Hedges, and M. R. James, Analysis of the operation of gradient echo memories using a quantum input-output model, New J. Phys. **15**, 085020 (2013).

[35] C. M. Caves and B. L. Schumaker, New formalism for two-photon quantum optics. I. Quadrature phases and squeezed states, Phys. Rev. A **31**, 3068 (1985).

[36] B. L. Schumaker and C. M. Caves, New formalism for two-photon quantum optics. II. Mathematical foundation and compact notation, Phys. Rev. A **31**, 3093 (1985).

[37] A. J. Shaiju and I. R. Petersen, A frequency domain condition for the physical realizability of linear quantum systems, IEEE T. Automat. Contr. **57**, 2033 (2012).

[38] H. J. Kimble, Y. Levin, A. B. Matsko, K. S. Thorne, and S. P. Vyatchanin, Conversion of conventional gravitational-wave interferometers into quantum nondemolition interferometers by modifying their input and/or output optics, Phys. Rev. D **65**, 022002 (2001).

[39] U. Leonhardt and A. Neumaier, Explicit effective Hamiltonians for general linear quantum-optical networks, J. Opt. B: Quantum Semiclass. Opt. **6**, L1 (2003).

[40] R. W. Boyd, *Padé Approximants* (Cambridge University Press, Cambridge, 1996), 2nd ed.

[41] Y. Chen, Macroscopic quantum mechanics: Theory and experimental concepts of optomechanics, J. Phys. B: At. Mol. Opt. Phys. **46**, 104001 (2013).

[42] J. Mizuno, Comparison of optical configurations for laser interferometric gravitational wave detectors, Thesis (1995).

[43] C. W. Gardiner and P. Zoller, *Quantum Noise: A Handbook of Markovian and Non-Markovian Quantum Stochastic Methods with Applications to Quantum Optics* (Springer, Berlin, 2004), 2nd ed.

[44] A. A. Clerk, M. H. Devoret, S. M. Girvin, F. Marquardt, and R. J. Schoelkopf, Introduction to quantum noise, measurement, and amplification, Rev. Mod. Phys. **82**, 1155 (2010).

[45] M. Aspelmeyer, T. J. Kippenberg, and F. Marquardt, Cavity optomechanics, Rev. Mod. Phys. **86**, 1391 (2014).

[46] C. M. Bender, Introduction to PT-symmetric quantum theory, Contemp. Phys. **46**, 277 (2005).

[47] B. de Schutter, Minimal state-space realization in linear system theory: an overview, J. Comput. Appl. Math. **121**, 331 (2000).

[48] W. Research, StateSpaceModel, https://reference.wolfram.com/language/ref/StateSpaceModel.html (2014), [Accessed: 20-June-2022].

[49] D. Luenberger, Canonical forms for linear multivariable systems, IEEE T. Automat. Contr. **12**, 290 (1967).

[50] W. Research, MinimalStateSpaceModel, https://reference.wolfram.com/language/ref/MinimalStateSpaceModel.html (2014), [Accessed: 20-June-2022].

[51] G. E. Antoniou, P. N. Paraskevopoulos, and S. J. Varoufakis, Minimal state-space realization of factorable 2-D transfer functions, IEEE T. Circuits Syst. **35**, 1055 (1988).

[52] A. Buonanno and Y. Chen, Scaling law in signal recycled laser-interferometer gravitational-wave detectors, Phys. Rev. D **67**, 062002 (2003).